RSC Advances

PAPER

Check for updates

A wrinkled structure of gold film greatly improves the signaling of electrochemical aptamer-based biosensors†

Shaoguang Li, [ID] [a] Lancy Lin,[b] Xueman Chang,[a] Zhixiao Si,[a] Kevin W. Plaxco, [ID] [cd] Michelle Khine,[b] Hui Li [ID] *[a] and Fan Xia [ID] [a]

Electrochemical aptamer-based (E-AB) sensors provide a great opportunity towards the goal of point-of-care and wearable sensing technologies due to their good sensitivity and selectivity. Nevertheless, the output signals from this sensor class remain low when sensors are interrogated *via* square-wave voltammetry. This low signaling limits the sensor's precision for its capability to detect small changes in target concentrations. To circumvent this, we proposed here the use of a readily shrink-induced, wrinkled Au-coating polyolefin film to immobilize a greater number of DNA probes and thus improve the signaling. Specifically, wrinkled gold film exhibits a 5.5-fold increase of surface area in comparison to the unwrinkled ones. Using these substrates we fabricated a set of E-AB sensors of three biological molecules, including kanamycin, doxorubicin and ATP. We achieved up to 10-fold increase in its current and also good accuracies within ±20% error in the target concentration range across 2 orders of magnitude.

Introduction

Electrochemical biosensors have received considerable attention towards the goal of point-of-care (POC) applications,[1–4] due to their high sensitivity, selectivity and capability of miniaturization.[5,6] Electrochemical aptamer-based (E-AB) sensors, for example, are a versatile platform supporting the detection of a broad range of targets irrespective of their chemical or enzymatic reactivity and thus including inorganic ions, proteins, small molecules and cells.[7–14] E-AB sensors are composed of a DNA/RNA or peptide aptamer "probe" that serves as a recognition element, and a covalently attached redox reporter which provides the readout signal. Upon undergoing a binding-induced conformational change, the electron transfer rate of the redox reporter is altered, thus providing an easily measurable electrochemical signal that is monotonically related to target concentration. Given this signaling mechanism, E-AB sensors are selective enough to

[a]Engineering Research Center of Nano-Geomaterials of Ministry of Education, Faculty of Materials Science and Chemistry, China University of Geosciences, Wuhan 430074, China. E-mail: lihui-chem@cug.edu.cn

[b]Department of Biomedical Engineering, University of California, Irvine, Irvine, CA 92697, USA

[c]Department of Chemistry and Biochemistry, University of California Santa Barbara, Santa Barbara, California 93106, USA

[d]Center for Bioengineering, University of California Santa Barbara, Santa Barbara, California 93106, USA

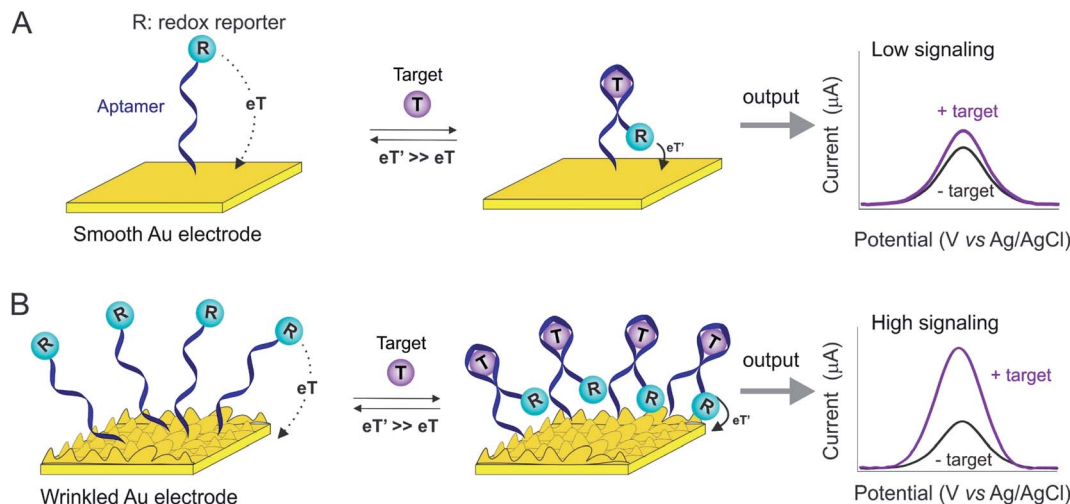† Electronic supplementary information (ESI) available. See DOI: 10.1039/d0ra09174j

be deployed in complex clinical samples and, even, *in situ* in the living body.[15,16]

The success of E-AB sensors notwithstanding, a limitation of this platform exists, *i.e.*, its low signaling output. This reflects as two aspects (Fig. 1). The first is low absolute current due to the fact that this is a voltametric approach, in which each redox reporter can provide very limited electrons (the methylene blue reporter most commonly employed is a two-electron redox process). This is in sharp contrast to enzymatic sensors, such as the continuous glucose sensor, in which each receptor catalytically turns over multiple copies of the target, producing many electrons/unite enzyme. Another reason for this low current is electrode surface with the limited macroscopic area, to which probes are allowed for attachment. Therefore, typical signaling currents from E-AB sensors that are small enough to insert *in vivo* are on the scale of microamperes or even nanoamperes.[17–20] This, in retrospect, limits the resolutions of sensors to determine small changes in target concentration. In order to enhance the signaling current of E-AB sensors, we and others have previously developed a set of electrochemical protocols that produce finely-controllable nanostructures on gold rod electrodes,[21–24] thus significantly enhancing their microscopic surface areas.[25–27] Building on this, here we explore the use of shrink-induced, wrinkled gold film substrates (Fig. S1†)[28,29] to greatly enhance the microscopic surface area of the sensing electrodes in E-AB sensors.

Fig. 1 The wrinkled structures of Au film greatly improve the surface area and thus E-AB sensor signaling. Typically, E-AB sensors are comprised of an immobilizing electrode (here, smooth or wrinkled gold electrode, Fig. S1†), DNA aptamers modified with redox reporter (labeled as "R") that covalently attached on the electrode. Target recognition alters the electron transfer kinetics of this reporter, and thus producing a measurable electrochemical signal output *via* square wave voltammetry. (A) Due to their limited microscopic surface area, fewer probes attach to a smooth gold electrode, thus limiting the signaling current. (B) The enhanced microscopic surface area of a wrinkled electrode, in contrast, increases the number of probes immobilize on a given macroscopic surface area, thus increasing the E-AB signaling current.

Experimental section

Materials

Tris(2-carboxyethyl)phosphine hydrochloride (TCEP), 6-mercapto-1-hexanol (MCH), and cocaine hydrochloride from Sigma-Aldrich (MO, USA); all were used as received. Polyolefin film was purchased from 0.5 mil seven-layer polyethylene/polypropylene blend, Sealed Air Corp. The methylene blue- and thiol-modified DNA aptamers were obtained from Sangon Biotech (Shanghai) Co., Ltd with HPLC purifications. These DNA sequences were dissolved in PBS buffer ($1\times$) (10.00 mM Na_2HPO_4; 1.75 mM KH_2PO_4; 137.00 mM NaCl; 2.65 mM KCl; pH = 7.4) to a final concentration of 100 μM, aliquoted and stored at -20 °C prior to use.

The DNA sequences used in this study are:

Kanamycin aptamer:

5′-HO-$(CH_2)_6$-S-S-$(CH_2)_6$-GGGACTTGGTTTAGGTAAT-GAGTCCC-$(CH_2)_7$-methylene blue (MB)-3′

Doxorubicin aptamer:

5′-HO-$(CH_2)_6$-S-S-$(CH_2)_6$-ACCATCTGTGTAAGGGG-TAAGGGGTGGT-$(CH_2)_7$-MB-3′

ATP aptamer (5′ to 3′):

5′-HO-$(CH_2)_6$-S-S-$(CH_2)_6$-ACC TGG GGG AGT ATT GCG GAG GAA GGT-$(CH_2)_7$-MB-3′

Gold film electrode fabrication

The unshrunk and shrunk Au-coating polyolefin films were fabricated following our previous study.[28,29] First, polyolefin films were cut into 70 mm × 70 mm squares and then adhered to silicon wafer substrates using 70% ethanol and Kapton tape. Next, a 40 nm of gold (Q150R S, Quorum Technologies) was deposited onto the above substrate, followed by subsequently photopatterned using Shipley 1827 (Microchem) positive resist

and UV exposure (MA6, Suss Microtec) *via* a photomask. Following this step, the wafers in I_2 : KI : H_2O (1 : 4 : 40) gold etchant was wet etched in order to remove the areas of gold that were exposed through the photolithographic patterning. Finally, acetone was applied to such surface to remove the remaining photoresist.

In order to obtain a well-defined gold geometric area, a polytetrafluoroethylene (PTFE) solution was applied to provide an insulation coating on the long gold electrodes, leaving only the hexagonal gold area for sensor immobilization. After drop-casting the Teflon solution on this substrate, it was left at ambient conditions for 30 minutes to dry out. With these, an unshrunk, planar gold film was obtained. To fabricate the shrunk, wrinkled electrode, the former film was baked in the oven at 150 °C for 5 min.

Sensor fabrication

To fabricate the E-AB sensors, an electrochemical cleaning process was applied for both planar and wrinkled substrates, with a slight difference between these two. For the unshrunk, planar film, we performed the surface area cleaning step to maintain the utility of film on such flexible substrate. Specifically, electrodes were immersed in 0.05 M sulfuric acid and scanned between 0 V and 1.65 V (all reported potentials are *versus* Ag/AgCl) for 16 segments using cyclic voltammetry. In contrast, the shrunk, wrinkled sensors required electrochemically roughening step in order to clean thoroughly. Briefly, these substrates were immersed in 0.5 M sulfuric acid and rapidly pulsed between $E_{initial} = 0.0$ V to $E_{high} = 2.0$ V for 400 000 times with each pulse being of 2 ms duration. Immediately prior to sensor fabrication a DNA solution in phosphate buffered saline buffer ($1\times$ PBS) (10.00 mM Na_2HPO_4; 1.75 mM KH_2PO_4 137.00 mM NaCl; 2.65 mM KCl; pH = 7.4) was prepared by

incubating a solution of 100 μM DNA and 20 mM tris-(2-carboxyethyl)phosphine hydrochloride (1 : 200) for 1 h at room temperature followed by dilution with PBS to 200 nM. DNA concentrations were confirmed by UV-Vis spectroscopy. Finally, freshly cleaned electrodes were immersed in this freshly-prepared DNA solution for 1 h at room temperature (for unshrunk, planar electrodes, the DNA solution was directly dropped on the surface to minimize the volume used). Finally, the sensors were rinsed with ultrapure water and then

incubated in 20 mM 6-mercapto-1-hexanol solution at room temperature for 3 h prior to use.

General protocol for electrochemical measurements

Electrochemical measurements were performed at room temperature using a multichannel CHI1040C potentiostat (CH Instruments, Austin, TX) and a standard three-electrode cell containing a platinum counter electrode and a Ag/AgCl (3 M KCl) reference electrode (Fig. S2, see the experimental setup in

Fig. 2 We characterized both planar and wrinkled electrode using scanning electron microscopy and electrochemical techniques. (A) The planar gold film is smooth and uniform; (B) in contrast, after shrinking, the film exhibits a complex, hierarchically wrinkled structure (see Fig. S2† the greater magnificent SEM for wrinkled electrode); (C) as expected, wrinkled gold film exhibits a 5.5-fold in surface area (red) of that observed for smooth gold film (black), which is in good accordance to our previous report.[20]
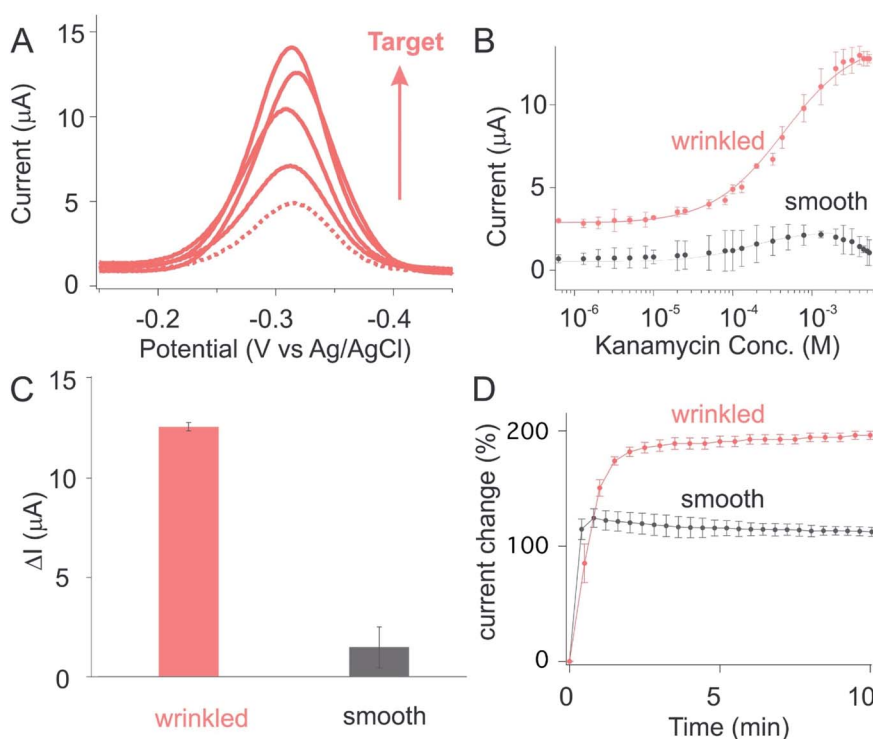

Fig. 3 A kanamycin-detecting electrochemical aptamer based (E-AB) sensor fabricated from wrinkled electrodes achieved a high signaling output. (A) As expected, we observed a monotonically increase of current (peak at −0.32 V) when spiking our sensors with increased target concentrations. The dotted line represents the voltammogram obtained from sensors in the absence of target. The subsequent voltammogram with increased current are collected from sensors spiked with a monotonical increase of target concentration (50 μM, 100 μM, 500 μM, 1 mM). (B) Prior to the addition of target, sensors fabricated on wrinkled electrode exhibit a 5-fold greater in absolute current for a given set of macroscopic dimensions (the size before shrunk: 70 mm × 70 mm, after shrunk: 14 mm × 14 mm). (C) The current difference between baseline (0 M target) and saturation (5 mM target), ΔI, is significantly enhanced by the use of wrinkled electrodes by 10-fold. (D) Sensors fabricated from either smooth or wrinkled electrodes respond rapidly to their target, reaching 90% of the total response within minutes (at, as shown here, 1 mM target), with wrinkled showing a slightly slower response probably due to slower diffusion onto the finely hierarchical structure. The error bars here and in the following figures represent the standard deviation of at least three independently fabricated sensors.
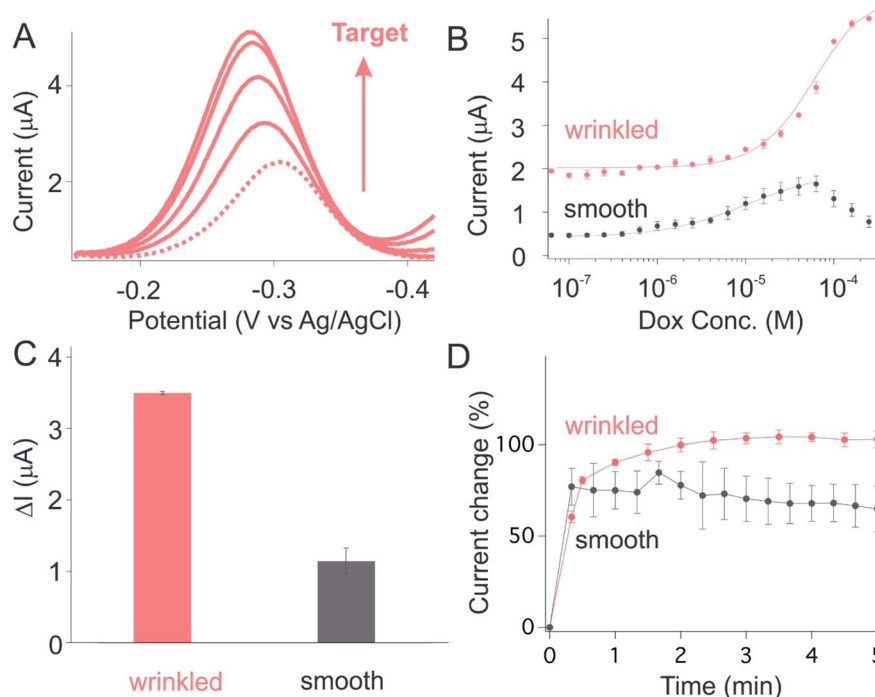
Fig. 4 A doxorubicin-detecting electrochemical aptamer based (E-AB) sensor fabricated from wrinkled electrodes achieved a high signaling output. (A) As expected, we observed a monotonically increase of current (peak at −0.30 V) when spiking our sensors with increased target concentrations. The dotted line represents the voltammogram obtained from sensors in the absence of target. The subsequent voltammogram with increased current are collected from sensors spiked with a monotonical increase of target concentration (5 μM, 10 μM, 25 μM, 40 μM). (B) Prior to the addition of target, sensors fabricated on wrinkled electrode exhibit a much greater absolute current for a given set of macroscopic dimensions (the size before shrunk: 70 mm × 70 mm, after shrunk: 14 mm × 14 mm). (C) The current difference between baseline (0 M target) and saturation (300 μM target), ΔI, is significantly enhanced by the use of wrinkled electrodes. (D) Sensors fabricated from either smooth or wrinkled electrodes respond rapidly to their target, reaching 90% of the total response within minutes (at, as shown here, 100 μM target), with wrinkled showing a slightly slower response probably due to slower diffusion onto the finely hierarchical structure.

ESI†). Square wave voltammetry (SWV) was performed using a potential window of −0.1 to −0.5 V, a potential step of 0.001 V, a frequency of 500 Hz and an amplitude of 0.05 V. All measurements in the kinetic and titration study was conducted after 30 scans in PBS buffer to desorption the DNA sequences that is non-specifically attached on the electrode surface.

Target kinetics and titration measurements

Kinetics measurements were conducted using the protocol as following: a set of freshly-prepared sensors were interrogated at a non-target solution to obtain the baseline current. Next, the sensors were spiked with a known target concentration followed by immediate and high-frequency electrochemical measurements at a time interval of 10–20 seconds. Comparing these current signals after target spiking with the baseline current, we obtained the kinetics curves for each type of sensor. Titration measurements were performed by spiking the sensors with a monotonically increased target concentrations at a time interval of 2 minutes to promise the probes reaching their equilibrium before interrogating.

Results

As our proof-of-principle study, we employed here two sets of gold-coating polyolefin flexible substrates (before and after heat-

shrink) to demonstrate their use in E-AB sensor application, with the detailed fabrication process and characterization reported in our previous studies.[28,29] As expected, before shrinking the gold film (70 mm × 70 mm in size) exhibited a smooth, uniform surface (Fig. 2A). After shrinking, in contrast, the electrode (14 mm × 14 mm in size) observed a hierarchical wrinkled structure (Fig. 2B), with plentiful, small winkle features of 20–30 μm, in good accordance with previous observations.[20] As determined by cyclic voltammetry measurements (Fig. 2C), the microscopic surface area of the wrinkled electrodes is enhanced 5.5-fold relative to that of the smooth electrodes.

Following on this, we then investigated the sensor performance of E-AB sensors fabricated using these wrinkled gold films, with the hypothesis that such structure will improve signaling. To see this, we first fabricated sensors against kanamycin, an antibiotic characterized by a narrow therapeutical window and significant potential for toxicity (leading to kidney failure and hearing loss).[30–32] As expected, we observed a monotonically increase in current when we challenged the sensor with increasing concentrations of kanamycin (Fig. 3A). The same data presented as a target titration curve produces the monotonic Langmuir isotherm behavior expected for this type of binding event (red curve, Fig. 3B). In comparison to the sensors fabricated using smooth gold film, we observed a greatly improved current change for sensors fabricated from shrunk, wrinkled electrode

(Fig. 3B). While the former produce current changes in the order of 0.1 μA upon the spike of saturated target. The wrinkled sensors, in contrast, exhibit a 10-fold enhancement in current change (Fig. 3C and S4†). Such enhancement is achieved only with slightly loss in its target binding kinetics (Fig. 3D), with both planar and wrinkled sensors reaching their 90% equilibrium at time scale of minutes.

To ascertain the generality of this approach to improving E-AB signaling current we next applied it to a doxorubicin-detecting sensor. As expected, we observed a monotonically increase in current when we challenge sensors built using either smooth or wrinkled electrode with increasing doxorubicin (Dox) concentrations (Fig. 4A and B). Once again, in comparison to the sensors fabricated from smooth electrodes, we observed improved current change for sensors fabricated from wrinkled electrodes (Fig. 4B). While sensors fabricated from planar electrodes exhibited current change in the order of 1.0 μA upon spiking saturated target, the wrinkled sensors in contrast exhibit a 3.5-fold enhancement in current change (Fig. 4C and S4†). Such enhancement is achieved only with slightly loss in its target binding kinetics, with both planar and wrinkled sensors reaching their 90% equilibrium at time scale of minutes (Fig. 4D).

As a third example we fabricated an ATP-detecting sensor using wrinkled gold electrodes. As expected, we observed

a monotonically increase in current when spiked with a set of ATP doses (Fig. 5A), producing the monotonic Langmuir isotherm behavior expected for this type of binding event (denoted as wrinkled, Fig. 5B). Once again, in comparison to the sensors on smooth electrode, we observed a greatly improved current change for sensors fabricated from wrinkled electrode (Fig. 5B and C). Specifically, while sensors on planar electrodes exhibit the absolute current change in the order of 1.0 μA upon spiking with saturated target, sensors fabricated from wrinkled substrate in contrast exhibit a 4.5 μA current change, a 4.5-fold of that observed for the former (Fig. 5C and S4†). Such enhancement is achieved only with slightly loss in its target binding kinetics (Fig. 5D), with both unshrunk and shrunk sensors reaching their 90% equilibrium at time scale of minutes.

The significantly improved signaling of E-AB sensors fabricated from wrinkled electrodes renders themselves to achieve good signal-to-noise ratio and thus high-precision measurements. To see this, we used titration fits from these three classes of sensors (Fig. 3B to 5B) to estimate the recovered concentrations from another sets of sensors out from the titration set. Specifically, we first used the Hill equation (eqn (1)) to fit the titration curves to derive the correlation between target concentration and electrochemical signal, here, the current obtained *via* a SWV techinque.
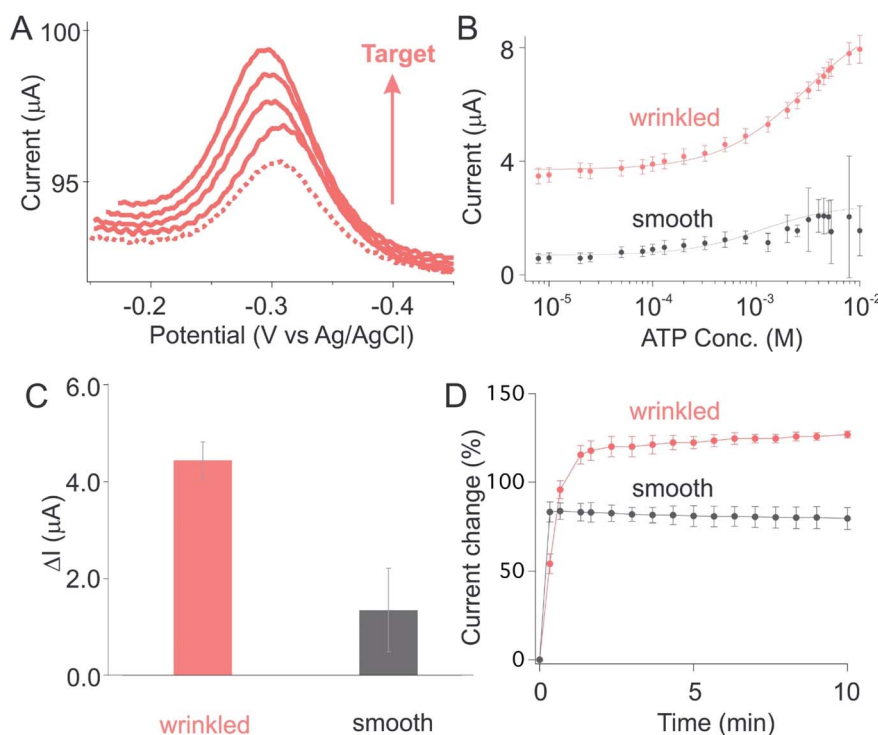

Fig. 5 An ATP-detecting electrochemical aptamer based (E-AB) sensor fabricated from wrinkled electrodes achieved a high signaling output. (A) As expected, we observed a monotonically increase of current (peak at −0.30 V) when spiking our sensors with increased target concentrations. The dotted line represents the voltammogram obtained from sensors in the absence of target. The subsequent voltammogram with increased current are collected from sensors spiked with a monotonical increase of target concentration (50 μM, 1.5 mM, 2.5 mM, 4 mM). (B) Prior to the addition of target, sensors fabricated on wrinkled electrode exhibit a much greater absolute current for a given set of macroscopic dimensions (the size before shrunk: 70 mm × 70 mm, after shrunk: 14 mm × 14 mm). (C) The current difference between baseline (0 M target) and saturation (10 mM target), Δ*I*, is significantly enhanced by the use of wrinkled electrodes. (D) Sensors fabricated from either smooth or wrinkled electrodes respond rapidly to their target, reaching 90% of the total response within minutes (at, as shown here, 10 mM target), with wrinkled showing a slightly slower response probably due to slower diffusion onto the finely hierarchical structure.
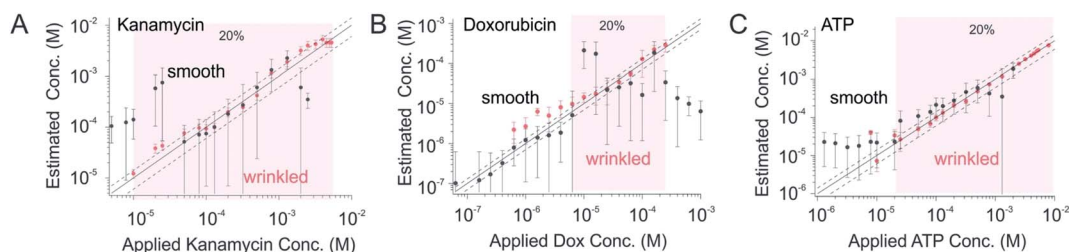
Fig. 6 The greatly improved signaling of wrinkled sensors achieved molecular measurements with high-precision. (A) Kanamycin-detecting sensors fabricated from wrinkled substrate are accurate to within ±20% (*i.e.*, the estimated concentration is within 20% of the spiked concentration) over the concentration range 10 μM to 6 mM (light pink). The planar sensors, in contrast, exhibited a much worse signal-to-noise ratio and failed in its accuracy. The dashed lines in all three panels represent ±20% error bands. (B) Doxorubicin-detecting sensors fabricated from wrinkled substrate are accurate to within ±20% (*i.e.*, the estimated concentration is within 20% of the spiked concentration) over the concentration range 6 μM to 300 μM (light pink). The planar sensors, in contrast, fallout from the accurate window due to their unsatisfied signaling. (C) Last, as a third example, ATP-detecting sensors fabricated from wrinkled substrate are accurate to within ±20% (*i.e.*, the estimated concentration is within 20% of the spiked concentration) over the concentration range 20 μM to 8 mM (light pink). The planar sensors, in contrast, fallout from the accurate window due to their unsatisfied signaling.

$$i = i_{\min} + (i_{\max} - i_{\min}) \frac{[\text{target}]^{n_{\mathrm{H}}}}{\left(K_{1/2}{}^{n_{\mathrm{H}}} + [\text{target}]^{n_{\mathrm{H}}}\right)} \quad (1)$$

where i is the current for sample measurement; $i_{\min}$, $i_{\max}$ are currents of sensors in the absence of target and in the presence of saturated target, respectively; n_{H} is the Hill coefficient; and $K_{1/2}$ is the midpoint of the binding curve for the sensor class. Once we have obtained these parameters target concentration can be defined from measurements of i alone using eqn (2), a recast form of eqn (1):

$$[\text{Target}] = K_{1/2}{}^{n_{\mathrm{H}}} \sqrt{\frac{i - i_{\min}}{i_{\max} - i}} \quad (2)$$

With this, we found that sensors fabricated from wrinkled electrode exhibited a greatly improved recovery rate in comparison to those fabricated from smooth ones. Kanamycin-detecting sensors fabricated from wrinkled electrode, for example, exhibited excellent precision to within ±20% (*i.e.*, the estimated concentration is within 20% of the spiked concentration) over the concentration range 10 μM to 6 mM (light pink) (Fig. 6A). In contrast, sensors fabricated from unshrunk, smooth gold film exhibited a 5-fold decrease in sensor precisions, *i.e.*, the standard deviations. Likewise, doxorubicin-detecting sensors fabricated from wrinkled electrodes are accurate to within ±20% over the concentration range 6 μM to 300 μM (light pink, Fig. 6B), in comparison to sensors on smooth substrate exhibiting a 4-fold decrease in precisions. The third example, ATP-recognizing sensors fabricated from wrinkled gold film are likewise accurate to within ±20% across 400-fold concentration range from 20 μM to 8 mM, in comparison to those on smooth substrate exhibiting a 2-fold decrease in precision in the same concentration range due to their unsatisfied signal-to-noise ratio.

substrates for E-AB sensors to achieve precise molecular measurements. Specifically, due to the increased surface area, such wrinkled structural gold film greatly improved the sensor signaling when spiking our E-AB sensors with their relevant targets, with a significant improvement range up to 10-fold. This achievement allows the sensors fabricated from wrinkled gold film to achieve a precise, accurate molecular measurements across a wide range of target spans. In contrast, the sensors fabricated from the pristine, smooth film exhibit a lower signal-to-noise ratio, rendering them incapable to determine their relevant target analytes with satisfied precisions.

Polyolefin, the polymer film we employed in our study as substrate, offers its excellent ability of thermal shrinkable, and thus they are commonly used to fabricate micro- and nano-structured materials. This provides an inspiring guideline to a broad range of other flexible polymers that have been recently employed in POC diagnostics. Heating-induced hierarchical structures, for example, can be applicable to improve signaling for sensors beyond electrochemical platform[33,34] such as photonic crystal-based sensing,[35] surface plasmon resonance (SPR),[36] or photonic nanosensing.[37] More significantly, this platform we proposed here is readily modular, so much that we could achieve molecular measurement against any analyte of interest simply by the replacement of its recognition element "aptamer" *via* a "plug and play" fashion. Given these, we believe our platform would provide new opportunity towards next-generation of point-of-care testing and wearable sensors.

Conflicts of interest

There are no conflicts to declare.

Acknowledgements

Conclusions

Here in this study we have demonstrated the use of a readily-prepared, heating-induced wrinkled gold film as immobilizing

References

1 Y. Yang and W. Gao, *Chem. Soc. Rev.*, 2019, **48**, 1465.

2 M. Bariya, H. Y. Y. Nyein and A. Javey, *Nat. Electron.*, 2018, **1**, 160.

3 D. N. Mazaafrianto, A. Ishida, M. Maeki, H. Tani and M. Tokeshi, *ACS Omega*, 2018, **3**, 16823.

4 Y. Zhou, Y. J. Yang, X. Deng, G. M. Zhang, Y. Zhang, C. H. Zhang, S. M. Shuang, Y. J. He and W. Sun, *Sens. Actuators, B*, 2018, **276**, 204.

5 H. Li, S. G. Li, J. Dai, C. C. Li, M. Zhu, H. X. Li, X. D. Lou, F. Xia and K. W. Plaxco, *Chem. Sci.*, 2019, **10**, 10843.

6 W. Z. Jia, A. J. Bandodkar, G. Valdes-Ramirez, J. R. Windmiller, Z. J. Yang, J. Ramirez, G. Chan and J. Wang, *Anal. Chem.*, 2013, **85**, 6553.

7 H. Li, N. Arroyo-Curras, D. Kang, F. Ricci and K. W. Plaxco, *J. Am. Chem. Soc.*, 2016, **138**, 15809.

8 A. A. Lubin and K. W. Plaxco, *Acc. Chem. Res.*, 2010, **43**, 496.

9 D. Kang, S. Sun, M. Kurnik, D. Morales, F. W. Dahlquist and K. W. Plaxco, *J. Am. Chem. Soc.*, 2017, **139**, 12113.

10 S. Li, C. Li, Y. Wang, H. Li and F. Xia, *Anal. Chem.*, 2020, **92**, 13427.

11 H. Li, J. Somerson, F. Xia and K. W. Plaxco, *Anal. Chem.*, 2018, **90**, 10641.

12 L. F. Fan, G. Z. Wang, W. T. Liang, W. J. Yan, Y. J. Guo, S. M. Shuang, C. Dong and Y. P. Bi, *Biosens. Bioelectron.*, 2019, **145**, 111728.

13 B. S. He, L. Wang, X. Z. Dong, X. H. Yan, M. Li, S. S. Yan and D. D. Yan, *Food Chem.*, 2019, **300**, 125179.

14 H. Jin, R. J. Gui, X. H. Gao and Y. J. Sun, *Biosens. Bioelectron.*, 2019, **145**, 111732.

15 N. Arroyo-Curras, J. Somerson, P. A. Vieira, K. L. Ploense, T. E. Kippin and K. W. Plaxco, *Proc. Natl. Acad. Sci. U. S. A.*, 2017, **114**, 645.

16 H. Li, P. Dauphin-Ducharme, N. Arroyo-Curras, C. H. Tran, P. A. Vieira, S. G. Li, C. Shin, J. Somerson, T. E. Kippin and K. W. Plaxco, *Angew. Chem., Int. Ed.*, 2017, **56**, 7492.

17 M. Roushani and K. Ghanbari, *Microchim. Acta*, 2019, **186**, 115.

18 X. Y. Wang, F. X. Gao, Y. Y. Gong, G. T. Liu, Y. Zhang and C. F. Ding, *Talanta*, 2019, **205**, 120140.

19 X. Y. Wang, Y. Q. Shan, M. Gong, X. Jin, L. R. Lv, M. Jiang and J. Xu, *Sens. Actuators, B*, 2019, **281**, 595–601.

20 D. Zhang, J. J. Ma, X. W. Meng, Z. F. Xu, J. Zhang, Y. X. Fang and Y. Guo, *Anal. Chim. Acta*, 2019, **1076**, 55–63.

21 N. Arroyo-Curras, K. Scida, K. L. Ploense, T. E. Kippin and K. W. Plaxco, *Anal. Chem.*, 2017, **89**, 12185.

22 L. Soleymani, Z. C. Fang, E. H. Sargent and S. O. Kelley, *Nat. Nanotechnol.*, 2009, **4**, 844.

23 L. L. Coria-Oriundo, H. Ceretti, Y. Roupioz and F. Battaglini, *ChemistrySelect*, 2020, **5**, 11391.

24 Z. Li, G. Dai, F. F. Luo, Y. Q. Lu, J. W. Zhang, Z. H. Chu, P. G. He, F. Zhang and Q. J. Wang, *Microchim. Acta*, 2020, **187**, 415.

25 S. Mahshid, A. H. Mepham, S. S. Mahshid, I. B. Burgess, T. S. Safaei, E. H. Sargent and S. O. Kelley, *J. Phys. Chem. C*, 2016, **120**, 21123.

26 G. A. Tig and S. Pekyardimci, *Talanta*, 2020, **210**, 120666.

27 Y. Zhang, J. Jiang, Y. F. Liu, P. Li, Y. Liu, L. J. Chen and J. W. Zhao, *Nanoscale*, 2020, **12**, 10842–10853.

28 A. Hauke, L. S. S. Kumar, M. Y. Kim, J. Pegan, M. Khine, H. Li, K. W. Plaxco and J. Heikenfeld, *Biosens. Bioelectron.*, 2017, **94**, 438.

29 J. D. Pegan, A. Y. Ho, M. Bachman and M. Khine, *Lab Chip*, 2013, **13**, 4205.

30 A. A. Rowe, E. A. Miller and K. W. Plaxco, *Anal. Chem.*, 2010, **82**, 7090.

31 C. M. C. Lu, S. H. James and Y. H. H. Lien, *Am. J. Kidney Dis.*, 1996, **28**, 767.

32 R. E. Black, W. K. Lau, R. J. Weinstein, L. S. Young and W. L. Hewitt, *Antimicrob. Agents Chemother.*, 1976, **9**, 956.

33 M. T. Holden, M. C. D. Carter, C. H. Wu, J. Wolfer, E. Codner, M. R. Sussman, D. M. Lynn and L. M. Smith, *Anal. Chem.*, 2015, **87**, 11420.

34 S. Lutz, P. Weber, M. Focke, B. Faltin, J. Hoffmann, C. Muller, D. Mark, G. Roth, P. Munday, N. Armes, O. Piepenburg, R. Zengerle and F. von Stetten, *Lab Chip*, 2010, **10**, 887.

35 J. Qin, X. Li, L. Cao, S. Du, W. Wang and S. Q. Yao, *J. Am. Chem. Soc.*, 2020, **142**, 417.

36 N. Cathcart and J. I. L. Chen, *Anal. Chem.*, 2020, **92**, 7373.

37 A. K. Yetisen, Y. Montelongo, F. D. Vasconcellos, J. L. Martinez-Hurtado, S. Neupane, H. Butt, M. M. Qasim, J. Blyth, K. Burling, J. B. Carmody, M. Evans, T. D. Wilkinson, L. T. Kubota, M. J. Monteiro and C. R. Lowe, *Nano Lett.*, 2014, **14**, 3587.